PDRs4All

Ilane Schroetter, Olivier Berné, Christine Joblin, Amélie Canin, Ryan Chown, Ameek Sidhu, Emilie Habart, Els Peeters, Thomas S.-Y. Lai, Alessandra Candian, et al.

A&A, 685, A78 (2024)
https://doi.org/10.1051/0004-6361/202348974

Astronomy & Astrophysics

PDRs4All

VII. The 3.3 μm aromatic infrared band as a tracer of physical properties of the interstellar medium in galaxies★

Ilane Schroetter[1], Olivier Berné[1], Christine Joblin[1], Amélie Canin[1], Ryan Chown[2,3], Ameek Sidhu[2,3], Emilie Habart[8], Els Peeters[2,3,4], Thomas S.-Y. Lai[9], Alessandra Candian[5], Shubhadip Chakraborty[6,7], Annemieke Petrignani[10], Boris Trahin[11], Dries Van De Putte[11], and Felipe Alarcón[12]

[1] Institut de Recherche en Astrophysique et Planétologie, Université Toulouse III – Paul Sabatier, CNRS, CNES, 9 Av. du colonel Roche, 31028 Toulouse Cedex 04, France
e-mail: ilane.schroetter@gmail.com
[2] Department of Physics & Astronomy, The University of Western Ontario, London, ON N6A 3K7, Canada
[3] Institute for Earth and Space Exploration, The University of Western Ontario, London ON N6A 3K7, Canada
[4] Carl Sagan Center, SETI Institute, 339 Bernardo Avenue, Suite 200, Mountain View, CA 94043, USA
[5] Anton Pannekoek Institute for Astronomy, University of Amsterdam, Amsterdam, The Netherlands
[6] Department of Chemistry, GITAM School of Science, GITAM Deemed to be University, Bangalore, India
[7] Institut de Physique de Rennes, UMR CNRS 6251, Université de Rennes 1, Campus de Beaulieu, 35042 Rennes Cedex, France
[8] Institut d'Astrophysique Spatiale, Université Paris-Saclay, CNRS, Bâtiment 121, 91405 Orsay Cedex, France
[9] IPAC, California Institute of Technology, Pasadena, CA, USA
[10] Molecular Photonics, Van 't Hoff Institute for Molecular Sciences, University of Amsterdam, Science Park 904, 1098 XH Amsterdam, The Netherlands
[11] Space Telescope Science Institute, Baltimore, MD 21218, USA
[12] Department of Astronomy, University of Michigan, Ann Arbor, MI 48109, USA

Received 15 December 2023 / Accepted 16 February 2024

ABSTRACT

Aromatic infrared bands (AIBs) are a set of broad emission bands at 3.3, 6.2, 7.7, 8.6, 11.2, and 12.7 μm, seen in the infrared spectra of most galaxies. With the *James Webb* Space Telescope (JWST), the 3.3 μm AIB can in principle be detected up to a redshift of ∼7. Relating the evolution of the 3.3 μm AIB to local physical properties of the interstellar medium (ISM) is thus of paramount importance. By applying a dedicated machine learning algorithm to JWST NIRSpec observations of the Orion Bar photodissociation region obtained as part of the PDRs4All Early Release Science (ERS) program, we extracted two template spectra capturing the evolution of the AIB-related emission in the 3.2–3.6 μm range, which includes the AIB at 3.3 μm and its main satellite band at 3.4 μm. In the Orion Bar, we analyzed the spatial distribution of the templates and their relationship with the ro-vibrational H_2 line at 2.12 μm, the pure rotational line of H_2 at 4.69 μm and the Pfund δ line at 3.29 μm. We find that one template (AIB_{Irrad}) traces regions of neutral atomic gas with strong far-UV fields, while the other template ($AIB_{Shielded}$) corresponds to shielded regions with lower FUV fields and a higher molecular gas fraction. We then show that these two templates can be used to fit the NIRSpec AIB-related spectra of nearby galaxies. The relative weight of the two templates ($AIB_{Irrad/Shielded}$) is a tracer of the radiative feedback from massive stars on the ISM. We derive an estimate of $AIB_{Irrad/Shielded}$ in a $z = 4.22$ lensed galaxy and find that it has a lower value than for local galaxies. This pilot study illustrates how a detailed analysis of AIB emission in nearby regions can be used to probe the physical conditions of the extragalactic ISM.

Key words. ISM: lines and bands – photon-dominated region (PDR) – galaxies: ISM

1. Introduction

Photodissociation regions (PDRs) are regions of the interstellar medium (ISM) where the far-ultraviolet (UV) photons ($6 < E < 13.6$ eV) from massive stars strongly influence the dust and gas. This deposition of energy results in the dissociation of molecules and the heating of the gas and dust. PDRs cool through emission in the infrared (IR). In the mid-IR wavelength range (3–28 μm), classic spectral signatures of PDRs are i) continuum emission attributed to dust grains, ii) H_2 emission lines, iii) emission lines from neutral atoms and ions ([S II], [Si II], etc.), and iv) aromatic infrared bands (AIBs), which are broad emission features generally attributed to fluorescent emission of large carbonaceous molecules such as polycyclic aromatic hydrocarbons (PAHs). The most prominent AIBs are found at wavelengths of 3.3, 6.2, 7.7, 8.6, 11.2, and 12.7 μm. Perhaps the main observational fact is that PAHs are ubiquitously observed in the interstellar medium (ISM) of star-forming galaxies (SFGs; e.g. Draine et al. 2007; Li 2020; Sandstrom et al. 2023), including at high redshift (e.g., Riechers et al. 2014; McKinney et al. 2020). PAHs are believed to play a major role in the physics and chemistry of PDRs and, notably, in heating the gas via the photoelectric effect (e.g. Bakes & Tielens 1994; Weingartner & Draine 2001; Berné et al. 2022a).

Here, we focus on the emission in the 3.2–3.6 μm range, which includes the AIB at 3.3 μm and less-prominent neighboring bands, in particular at 3.4 μm. While the emission at

★ Based on JWST ERS program #1288.

Table 1. Aperture parameters used to extract NIRSpec spectra from nearby galaxies.

Galaxy name (1)	Center RA (2)	Center Dec (3)	Radius ($l \times h$) (4)	$\text{Radius}_{\text{sub}}$ (5)	PA (6)
IIZw96	20:57:24.376	17:07:39.7	1.27×0.75	···	25
VV114	01:07:47.530	–17:30:25.30	0.51×0.38	0.13×0.08	33
NGC7469	23:03:15.633	8:52:26.21	0.79×0.79	···	0
NGC3256 nucl1	10:27:51.231	–43:54:14.00	0.34×0.34	0.06	0
NGC3256 nucl2	10:27:51.218	–43:54:19.42	0.38×0.24	0.06	20

Notes. (1) Galaxy name; (2) RA of the ellipse center (J2000); (3) DEC of the ellipse center (J2000); (4) radius of ellipse in kpc (semi-major and semi-minor axes); (5) radius of subtracted ellipse in kpc; (6) ellipse position angle (in degrees; same for both apertures).

3.3 μm is attributed to aromatic C–H stretching vibrations, the emission at 3.4 μm is attributed to aliphatic C-H stretching vibrations (e.g., Allamandola et al. 1989; Joblin et al. 1996; Yang et al. 2016). These bands are also seen in galaxy spectra (i.e., Li 2020, and references therein).

Kim et al. (2012) and Lai et al. (2020) showed that the 3.3 μm emission can be a reasonable star formation (SF) indicator, and Rigopoulou et al. (2021) demonstrated that PAH intensity ratios could be used to probe physical conditions of the ISM of galaxies and thus differentiate between normal SFGs and galaxies hosting an AGN. Using near-IR spectra of M82 observed by AKARI, Yamagishi et al. (2012) found that the spatial evolution of the spectra can be explained by two main components: the AIB at 3.3 μm and the aliphatic satellite band at 3.4 μm. The ratio between the intensity of the 3.3 and 3.4 μm bands seems to increase the closer to the galaxy AGN the observations are.

Observations with the *James Webb* Space Telescope (JWST) open up new possibilities for using these signatures to trace the physical conditions in galaxies. Indeed, first observations with the JWST have shown that the AIB at 3.3 μm and its satellite at 3.4 μm are observed and bright in galaxies of the nearby Universe (e.g., Evans et al. 2022; Inami et al. 2022; U et al. 2022; Lai et al. 2023) and up to a redshift of four (the lensed galaxy SPT0418-47; Spilker et al. 2023), where the only detected spectral feature in the galaxy spectrum is the AIB at 3.3 μm observed with JWST/MIRI MRS. In principle, this AIB could be detected up to a redshift $z \approx 7$ with MIRI MRS. It is therefore useful to understand how this emission is linked to local physical properties.

In this work, we used JWST-ERS NIRSpec observations of the Orion Bar (program ID # 1288; Berné et al. 2022b) to extract elementary spectra using a machine learning approach based on nonnegative matrix factorization (NMF) following previous studies (Berné et al. 2007; Foschino et al. 2019). The article is composed as follows: we describe the data in Sect. 2, and in Sect. 3, we detail the process of extracting the AIB templates in the near-IR (3.2–3.7 μm) range for the Orion Bar. We then compare these templates with the ones from Foschino et al. (2019). In Sect. 3.3, we analyze the spatial distribution of the templates and establish the relationship between these templates and the ISM properties in Sect. 3.4. We then use the templates to analyze galaxy spectra in Sect. 4, and we extend the method to the spectra of spatially resolved galaxies in Sect. 4.2. Finally, conclusions are presented in Sect. 5. Throughout the paper, we use a 737 cosmology ($H_0 = 70$ km s^{-1}, $\Omega_m = 0.3$, and $\Omega_\Lambda = 0.7$), and all errors are given at 1σ unless stated otherwise.

2. Data

2.1. Orion Bar

The observations were performed with the JWST-NIRSpec Integral Field Unit (IFU) as part of the PDRs4All ERS program (Berné et al. 2022b) on September 10, 2022. They were reduced using the JWST pipeline version 1.9.4 with the Calibration Reference Data System (CRDS) context file jwst_1014.pmap. For this study, we only used the spectral cube corresponding to the F290LP filter that spans from ~2.9 to 5 μm. This data cube is a combination of nine pointings, forming a mosaic spanning the Orion Bar. The detailed data reduction together with a general analysis of the line emission is described in Peeters et al. (2024) and in Chown et al. (2024), where a first description of the PAH emission is also discussed.

2.2. Galaxies

At the time of writing this paper, four galaxies from the ERS program #1328[1] have been observed with NIRSpec. Those galaxies are VV114 (Evans et al. 2022; Rich et al. 2023; Linden et al. 2023), NGC 7469 (U et al. 2022; Lai et al. 2022; Bohn et al. 2023; Armus et al. 2023; Lai et al. 2023; Bianchin et al. 2024), IIZw96 (Inami et al. 2022), and NGC 3256 nucleus 1 and nucleus 2. We retrieved the level 3 NIRSpec IFU cubes from MAST for these five pointings covering filters 100, 170, and 290LP. For each pointing, we extracted the average spectrum using elliptical apertures from the cubes (see Table 1). As most of the galaxies observed have saturated spectra near their center, we excluded the saturated area when extracting each galaxy spectrum.

We also include data for the M82 galaxy from the GO program id # 2677. These are NIRSpec MSA observations of the nucleus and disk edge with the F290LP filter. Here, we use the data for the nucleus only, since they provide the best detection of the AIB at 3.3 μm and its satellite band at 3.4 μm. We obtained a mean spectrum by averaging the spectra obtained in all shutters.

In addition, another ERS program (id # 1355) released their MIRI MRS reduced data of a redshift $z \approx 4$ galaxy, called SPT0418-47, in which the AIB at 3.3 μm is present (Spilker et al. 2023). For this specific galaxy, we followed the reduction process provided by the authors in order to extract a unique average spectrum of this lensed source for all channels of MIRI. In total, we thus obtained seven average spectra covering the range of the emission bands at 3.3 and 3.4 μm in near and far galaxies.

3. Template NIRSpec AIB-related spectra in the Orion Bar

3.1. Extracting template spectra from the observed data cube

Our aim is to extract a set of representative elementary (template) spectra from the observed NIRSpec spectral cubes of the Orion Bar. To do so, we followed the decomposition method presented in Boulais et al. (2021) and Foschino et al. (2019).

[1] Details of this program can be seen on their website: https://goals.ipac.caltech.edu/

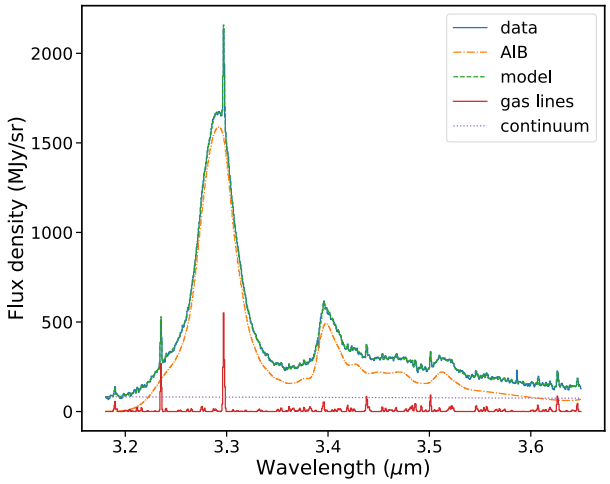

Fig. 1. Example of a spectrum of a spaxel of Orion Bar NIRSpec mosaic fitting. As the other 8690 spectra, this spectrum was extracted using an aperture with a radius of one pixel and was fit using a linear combination of Gaussians (AIB-related bands in orange), gas lines (in red), and continuum (in purple). The model can be seen in dashed green above the data shown in blue.

Details of the method are provided in these two references, but we briefly describe them here. First, the 3D NIRSpec data cube $C(\alpha, \delta, \lambda)$ is transformed into a 2D matrix: $X(m, \lambda)$, with $\dim(C) = (m_\alpha, m_\delta, n_\lambda)$ and $\dim(X) = (m, n_\lambda)$, $m = m_\alpha \times m_\delta$. In this study, we considered a wavelength range between $3.18 < \lambda < 3.65$ μm that covers the AIB at 3.3 μm and its satellite bands, in particular the major one at 3.4 μm. Then, we filtered out low signal-to-noise ratio (S/N) spectra in X using cutoffs in flux to remove potential spikes and saturated spectra in this wavelength range. Those cutoffs are the following: in each spectrum, intensities larger than 4×10^5 MJy sr^{-1} are set to 10^{-16}. This cutoff value was chosen to be larger than any real emission line in our data, and it corresponds to spikes present in the data. We then selected only those spectra the sum of whose values is greater than one (this removes spectra that contain no information at the border of the field of view). The selected spectra constitute the lines of the matrix X, which has dimensions of 8690, 706, that is, 706 spectral points and 8690 spatial positions. Spectra in X were then fit using a combination of synthetic components (AIB-related bands, gas lines, and continuum) in order to remove the contribution from gas lines and dust emission and extract the emission related to the AIBs (see Foschino et al. 2019 and Fig. 1). We define the matrix X^* whose lines are these 8690 pure AIB fit spectra (e.g., orange curve in Fig. 1). The next step consists of identifying the dimension of the subspace spanned by the data in X^*. This is done as in Boulais et al. (2021), by analysis of the eigenvectors of the covariance matrix. Using this method, we find that this dimension is $r = 2$. We then apply nonnegative matrix factorization (NMF; Lee & Seung 1999) to X^* with $r = 2$, which provides the matrices W and H, such that $X^* \approx WH$. Following Boulais et al. (2021), the NMF algorithm is initialized using the results of the MASS algorithm applied to X^*.

3.2. Extracted AIB-related spectra

The $r = 2$ extracted AIB-related spectra are presented in Fig. 2. The two spectra are similar; however, they show some specific differences. The first template spectrum ($\text{AIB}_{\text{Irrad}}$ hereafter) in red in Fig. 2 is dominated by a strong band at 3.294 μm and a weak band at 3.393 μm. An underlying plateau is present from ~3.36–3.53, but it is relatively weak compared to the 3.294 band. The second template spectrum ($\text{AIB}_{\text{Shielded}}$ hereafter) in blue in Fig. 2 shows a prominent band at 3.290 μm, which is broader than the same band in the $\text{AIB}_{\text{Irrad}}$ spectrum. The 3.4 μm emission feature in $\text{AIB}_{\text{Shielded}}$ is also much stronger. The template $\text{AIB}_{\text{Shielded}}$ also shows a more prominent plateau in the 3.36–3.53 μm range[2].

For each template, we estimate the 3.4–3.3 μm band intensity ratios. The 3.3 μm band intensity is obtained between 3.24 and 3.35 μm, and the 3.4 μm band between 3.38 and 3.42 μm. For each band, we subtract a linear continuum between the integration ranges to obtain only the band emission. The 3.4/3.3 integrated intensity band ratio is 0.04 for template $\text{AIB}_{\text{Irrad}}$ and 0.10 for template $\text{AIB}_{\text{Shielded}}$. These values correspond well to the extremes of this band ratio as derived from NIRSpec observations of NGC 7469 (Lai et al. 2023). As mentioned before, the 3.3 μm band is associated with aromatic C-H stretch emission, while the 3.4 μm band is attributed to aliphatic C-H emission (Allamandola et al. 1989). The fraction of aliphatics is found to be relatively minor (typically one methyl side group per PAH for $\text{AIB}_{\text{Shielded}}$ following Joblin et al. 1996 and Yang et al. 2016). If the carriers of the 3.4 μm band are over-hydrogenated PAHs rather than alkylated PAHs (Bernstein et al. 1996), then an even smaller amount of CH aliphatic bonds is required to explain the observed 3.4 to 3.3 μm band intensity ratios (Yang et al. 2020). In all cases, the $\text{AIB}_{\text{Irrad}}$ template corresponds to the emission of PAHs with very few attached aliphatic C–H bonds. Because the latter are more easily photodissociated than aromatic C–H bonds upon UV irradiation (Marciniak et al. 2021), the $\text{AIB}_{\text{Irrad}}$ spectrum can be regarded as corresponding to more UV-processed PAHs with respect to the $\text{AIB}_{\text{Shielded}}$ spectrum. On the contrary, the species emitting the $\text{AIB}_{\text{Shielded}}$ spectrum have been less exposed to UV irradiation (Joblin et al. 1996; Pilleri et al. 2015; Chown et al. 2024; Peeters et al. 2024), which was also recently seen in NGC7469 by Lai et al. (2023). In Fig. 3, we present both templates, together with two templates from Foschino et al. (2019) in the same wavelength range, ordered by visual ratio of the 3.3 over 3.4 μm bands. The $\text{AIB}_{\text{Shielded}}$ template is very close to the neutral PAH^0 template of Foschino et al. (2019) – yet with a slightly stronger 3.4 band, thus confirming that it corresponds to regions that are rather shielded from the UV or denser in which more pristine material is exposed to UV photons. The $\text{AIB}_{\text{Irrad}}$ template is close to the PAH^X template – yet with slightly more emission at 3.4 μm – which corresponds to the most irradiated environments.

3.3. Spatial distribution of the extracted templates

To complement this interpretation, we derived the spatial distribution of templates $\text{AIB}_{\text{Irrad}}$ and $\text{AIB}_{\text{Shielded}}$ spectra in the Orion Bar. To do this, we used a linear combination of the two template AIB-related spectra + gas lines + continuum to fit each of the observed spectrum at each spatial position in the NIRSpec cube (see details of the fitting method in Foschino et al. 2019). The respective contribution of the two AIB template spectra, which results from this fit, is shown in Fig. 2. The template $\text{AIB}_{\text{Irrad}}$ dominates in the northwest of the field of view, that is, in regions closer to the massive trapezium stars, while template $\text{AIB}_{\text{Shielded}}$ is found to be mostly present to the southeast of the field of view. $\text{AIB}_{\text{Shielded}}$ is also found to follow some dense structures present in the field of view of the Orion Bar, that is,

[2] Both templates can be found at https://doi.org/10.5281/zenodo.10776844

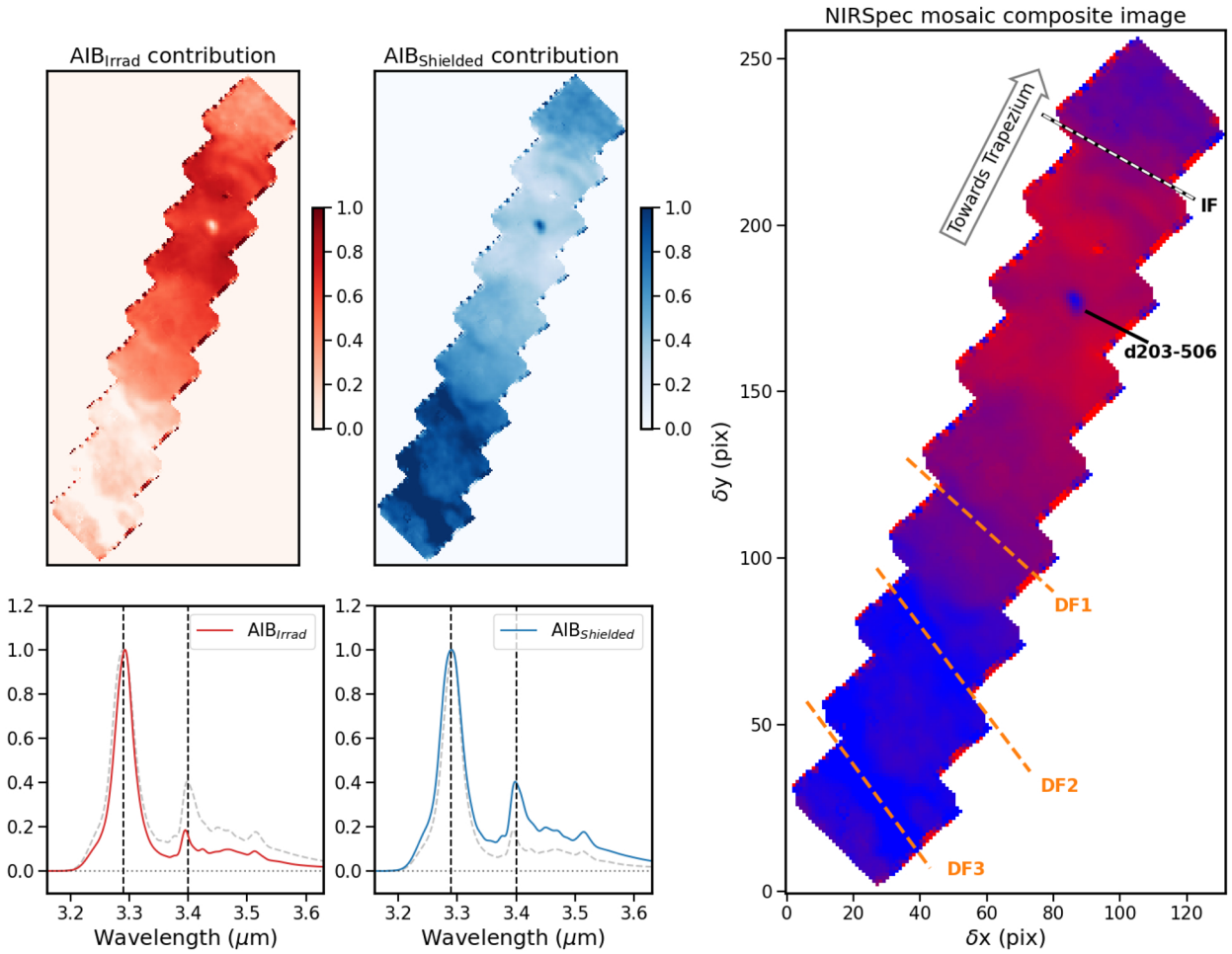

Fig. 2. Presentation and distribution of the two extracted template spectra. *Left column* : AIB$_{Irrad}$ map on top and the corresponding normalized template spectrum of the AIB$_{Irrad}$ component. *Middle column*: same as left column, but for the AIB$_{Shielded}$ template. We note that AIB$_{Irrad}$ has a more prominent 3.3 μm band (and a slightly redder peak) than AIB$_{Shielded}$, which has a stronger 3.4 μm band. For a quick comparison between both templates, on each bottom panel, the complementary template is shown in dashed gray lines. *Right column*: composite image of both AIB$_{Irrad}$ (red) and AIB$_{Shielded}$ (blue) contributions. The ionization front (IF) and the dissociation fronts (DF1, 2, and 3) are represented by dashed white and orange lines, respectively (defined in Habart et al. 2024 and Peeters et al. 2024).

the d203-506 protoplanetary disk (Berné et al. 2023) and several dense dissociation fronts seen in H_2 with NIRCam (Habart et al. 2024). The observed spatial distribution for templates AIB$_{Irrad}$ and AIB$_{Shielded}$ spectra is compatible with the photochemical scenario discussed above; namely, AIB$_{Irrad}$ traces the regions that are more exposed to UV photons, and AIB$_{Shielded}$ is more characteristic of denser and UV-shielded regions. In Fig. 2, however, we note that there is an excess in AIB$_{Shielded}$ beyond the ionization front in the HII region. This is most likely because the AIB emission in this upper corner of the map emanates from the background face-on PDR nebula and not the HII region itself (see Fig. 5 of Habart et al. 2024).

3.4. Relationship between the template AIB-related spectra and PDR physical properties

In order to assess the relationship between these templates and physical conditions in more detail, we extracted several quantitative parameters on each spaxel of the Orion Bar NIRSpec field of view. We derived AIB$_{Irrad/Shielded}$, the ratio of integrated intensity of the AIB$_{Irrad}$ template over the integrated intensity of the AIB$_{Shielded}$ template. We also extracted, for all pixels, the integrated intensities of the pure rotational H_2 0–0 S(9) line at $\lambda = 4.695$ μm, the H_2 1–0 S(1) ro-vibrational line at $\lambda = 2.122$ μm, the Pfund Hydrogen recombination line at $\lambda = 3.297$ μm, and the O I line at $\lambda = 1.317$ μm. This latter line emission results from UV-induced fluorescence, and it can be used to derive the intensity of the UV radiation field G_0 (see Peeters et al. (2024) and references therein). We thus followed the approach of these authors to estimate the distribution of G_0 (in units of the Habing 1968 field) within the NIRSpec field of view. Finally, we used the extracted integrated intensity of the AIB-related emission between 3.2 and 3.7 μm from Peeters et al. (2024), which is written I_{AIB}.

In Fig. 4, we plot AIB$_{Irrad/Shielded}$ as a function of the ratios between AIB emission and the H_2 line intensities, the ratio of the Pfund-δ Hydrogen recombination line at $\lambda = 3.297$ μm to the H_2 pure rotational line at $\lambda = 4.695$ μm, and the intensity of the UV radiation field derived from the O I line at $\lambda = 1.317$ μm. Strong variations of the AIB$_{Irrad/Shielded}$ ratio are observed, from $\sim 10^{-3}$ to ~ 5. Some outliers are present in this diagram with values >10, corresponding to the edge of the NIRSpec mosaic where the fit is poor. All ratios on the X-axis of the four panels in Fig. 4 have been chosen to increase in more irradiated regions. AIB$_{Irrad/Shielded}$ thus appears to be large in regions where the UV field is the strongest and where H_2 is photodissociated

Table 2. Properties of galaxies with spectroscopy in the 3.3 μm AIB range obtained as part of the GOALS and TEMPLATES JWST-ERS programs.

Galaxy name (1)	Redshift (2)	$I_{AIB}/H_2(4.69)$ (3)	$I_{AIB}/H_2(2.12)$ (4)	Pfund(3.29)/H_2(4.69) (5)	$AIB_{Irrad/Shielded}$ (6)	SFR (7)
IIZw96	0.0361[(1)]	59.2	40.3	1.3	0.488	40–60[(1)]
VV114	0.0202[(2,3)]	81.3	54.6	0.73	0.411	38[(4)]
NGC7469	0.01627[(5)]	135.1	73.5	0.97	1.067	10–30[(6)]
NGC3256 nucl1	0.009364[(7)]	217.4	89.3	2.6	0.689	30[(8)]
NGC3256 nucl2	0.009364[(7)]	69.4	32.7	2.5	0.412	50[(8)]
STP0418-47	4.2248[(9)]	≥64.9	≥59.2	≥5.8	0.075	350[(9)]
M82 nucleus	0.00073[(10)]	0.0061	···	···	0.741	10[(11)]

Notes. (1) Galaxy name; (2) galaxy redshift; (3) $I_{AIB}/H_2(4.69) = H_2(\lambda 4.6946)/(AIB_{3.2-3.7})$ flux ratio; (4) $I_{AIB}/H_2(2.12) = H_2(\lambda 2.1218)/(AIB_{3.2-3.7})$ flux ratio; (5) Pfund(3.29)/H_2(4.69) = Pfund(λ3.297)/$H_2(\lambda 4.6946)$ flux ratio; (6) $AIB_{Irrad/Shielded} = AIB_{Irrad}/AIB_{Shielded}$; (7) galaxy SFR (in $M_\odot$ yr^{-1}). [(1)]Inami et al. (2022); [(2)]Evans et al. (2022); [(3)]Rich et al. (2023); [(4)]Basu-Zych et al. (2013); [(5)]U et al. (2022); [(6)]Lai et al. (2022); [(7)]Yuan et al. (2019); [(8)]Sakamoto et al. (2014); [(9)]Spilker et al. (2023); [(10)]Morabito et al. (2014); [(11)]Yoast-Hull et al. (2013).

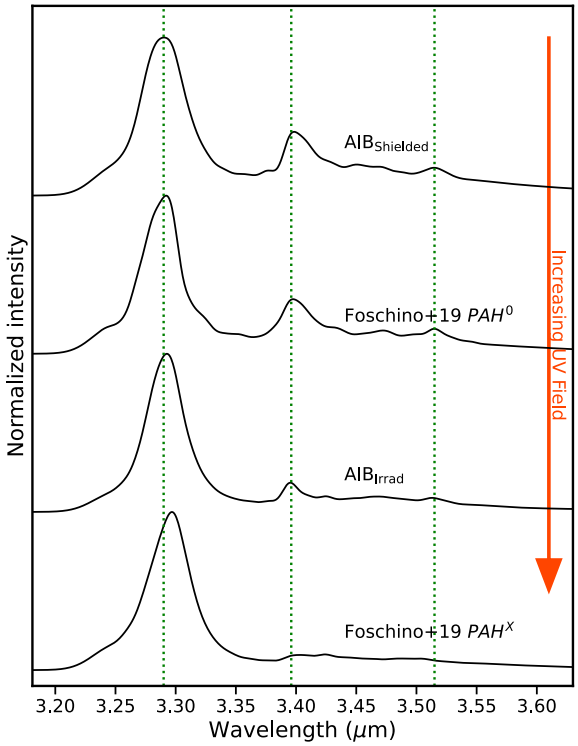

Fig. 3. Comparison of $AIB_{Shielded}$ (top) and AIB_{Irrad} (third position from top) with two templates of Foschino et al. (2019), namely PAH^0 (second position from top) and PAH^X (bottom). The order from top to bottom follows the increase in UV field intensity.

(but not the AIB carriers). $AIB_{Irrad/Shielded}$ is smaller in regions of lower UV field, where H_2 can form and thus the AIB-to-H_2 ratio is smaller. Similarly, $AIB_{Irrad/Shielded}$ is larger in regions where the Pfund-δ (ionized gas) over H_2 (warm molecular gas) ratio is large. Finally, this trend is also observed with a radiation field; that is, $AIB_{Irrad/Shielded}$ increases with the intensity of the radiation field as derived from the O I line. More specifically, the points with the top 10% of $AIB_{Irrad/Shielded}$ ratios have a median $G_0 = 2.0 \times 10^4$, while those with the bottom 10% $AIB_{Irrad/Shielded}$ratio have a median $G_0 = 4.9 \times 10^3$. We note that this approach only allows us to probe the intensity of the radiation field, while the hardness could also play a role on the AIB-derived ratio (see Yang & Li 2023). The effect of hardness could be tested by observing several PDRs illuminated by stars with various masses. The increase of $AIB_{Irrad/Shielded}$ is steep in the range where the AIB to H_2 ratio is comprised between a few 10s and 2×10^2, and then much shallower beyond this latter value, creating a "shoulder" in the diagrams in the upper panels of Fig. 4. This shoulder corresponds to spectra at the dissociation fronts present in the Orion Bar (DF1, DF2, DF3; see Fig. 2). Overall, these results support the interpretation in Sects. 3.2 and 3.3 related to the processing of the AIB carriers with UV field inside the PDR.

4. Application to galaxies

4.1. Fitting global galaxy spectra using the templates

We now turn to galaxies observed with NIRSpec. We fit the seven average spectra of these objects in our sample using a linear combination of emission lines, continuum, and both AIB_{Irrad} and $AIB_{Shielded}$ templates (we followed the same procedure as in Sect. 3.3, but accounting for galaxy redshift when fitting the spectra). For galaxy SPT0418-47, as the spectrum has a relatively low S/N (≈2), emission lines are not detected and thus not included in the fit.

Figure 5 shows all the fits obtained for nearby galaxies. The root-mean-square normalized error (see definition, e.g., in Boulais et al. (2021)) is below 1%. From those fits, we extracted the $AIB_{Irrad/Shielded}$ and compared them to the same observational parameters as for the Orion Bar (Fig. 4). For all galaxies in the study, the derived values overlap with those of the Orion Bar. Interestingly, for all the nearby galaxies, the points are situated near the shoulder of the Orion Bar data. This indicates that the AIB spectra from those nearby galaxies likely trace the irradiated surfaces of molecular clouds in the vicinity of massive stars. As can be seen in the bottom right panel of Fig. 4, the range of values of $AIB_{Irrad/Shielded}$ derived for nearby galaxies is consistent with a radiation field in the range of $G_0 \sim 2$–20×10^3 (Fig. 4). Properties and results for those galaxies are listed in Table 2.

4.2. Fitting the spectra of spatially resolved galaxies

In order to obtain complementary insights into the variations of the AIB emission within local galaxies, we now perform a similar analysis by fitting the spectra at all spatial positions within

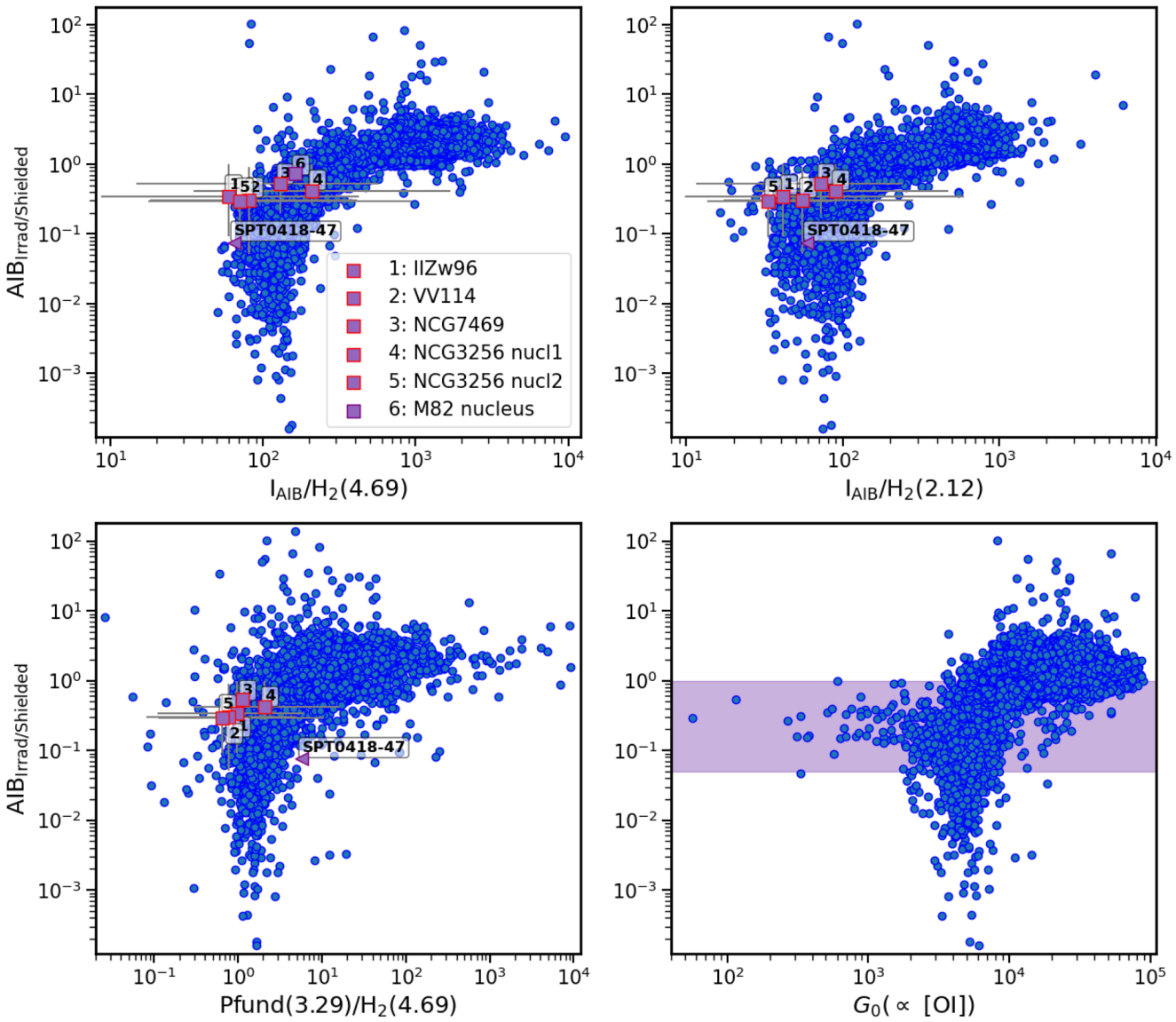

Fig. 4. $AIB_{Irrad/Shielded}$ as function of I_{AIB}/H_2 flux ratio for the rotational H_2 0–0 S(9) emission line at $\lambda \approx 4.69$ μm (top left panel) and the ro-vibrational H_2 1–0 S(1) emission line at $\lambda \approx 2.12$ μm (top-right panel). We note that for M82, we only have access to $H_2(4.69)$ as there is no observation available of $H_2(2.12)$ emission line in NIRSpec yet. The bottom row shows the same ratio as a function of Pfund($\lambda \approx 3.29$ μm)/$H_2(\lambda \approx 4.69$ μm) in the left panel and of G_0 in the right panel. For G_0, in purple, we indicate the area of $AIB_{Irrad/Shielded}$ corresponding to galaxies. For all panels, blue circles are the Orion Bar NIRSpec values for each spaxel. Purple squares represent the positions of the galaxies studied in these diagrams. Spatially resolved galaxies are represented with a red edge and have error bars corresponding to 1 σ percentiles (5% and 95% of fit values for all galaxy spaxels). For these points, the median values of all the fits are shown.

the NIRSpec cubes of the GOALS program[3]. The fitted spectra are extracted over an aperture of one pixel radius. We thus obtained approximately 1500 spectra per pointing. Each spectrum is then fit using the linear combination of the extracted templates (AIB_{Irrad} and $AIB_{Shielded}$, linear and power-law continuum, and emission lines), as above. From these fits, we derive the maps of the $AIB_{Irrad/Shielded}$ ratio for each galaxy. Those maps are shown in Fig. 6. In this figure, we also include the maps of the Paschen alpha line at 1.875 μm (left column) and of the integrated intensity of the 3.3 μm AIB. Emission in the Paschen alpha line is a tracer of extreme UV ($E > 13.6$ eV) photons, while the 3.3 μm integrated intensity is more sensitive to far-UV ($E < 13.6$ eV) photons. Thus, both are tracers of the radiative feedback from OB stars in the ISM, yet with different physical conditions (respectively, HII region vs. PDR; Peeters et al. 2024). Since the evolution of the ratio of the 3.3 over 3.4 μm bands and, therefore, the relative contribution of AIB_{Irrad} and $AIB_{Shielded}$ depend on the FUV intensity (Joblin et al. 1996, Fig. 3 of this work), in Fig. 6 we compare the spatial distribution of $AIB_{Irrad/Shielded}$ with that of the 3.3 μm band.

In the case of IIZw96, $AIB_{Irrad/Shielded}$ seems to follow the Paschen alpha and the 3.3 μm emissions at first glance. However, when observing in more detail, the $AIB_{Irrad/Shielded}$ ratio peaks near the central Paschen alpha and 3.3 μm knots, but not necessarily exactly at their positions. Also, some knots are seen peaking in Pa alpha and 3.3 emission but not in $AIB_{Irrad/Shielded}$. In VV114, $AIB_{Irrad/Shielded}$ is bright in the northeastern knot of 3.3 μm and Paschen alpha emission, but it is small near the

[3] For M82, however, this galaxy has no NIRSpec IFU observation available, and we thus cannot perform a "resolved" fitting as with the other five nearby galaxies.

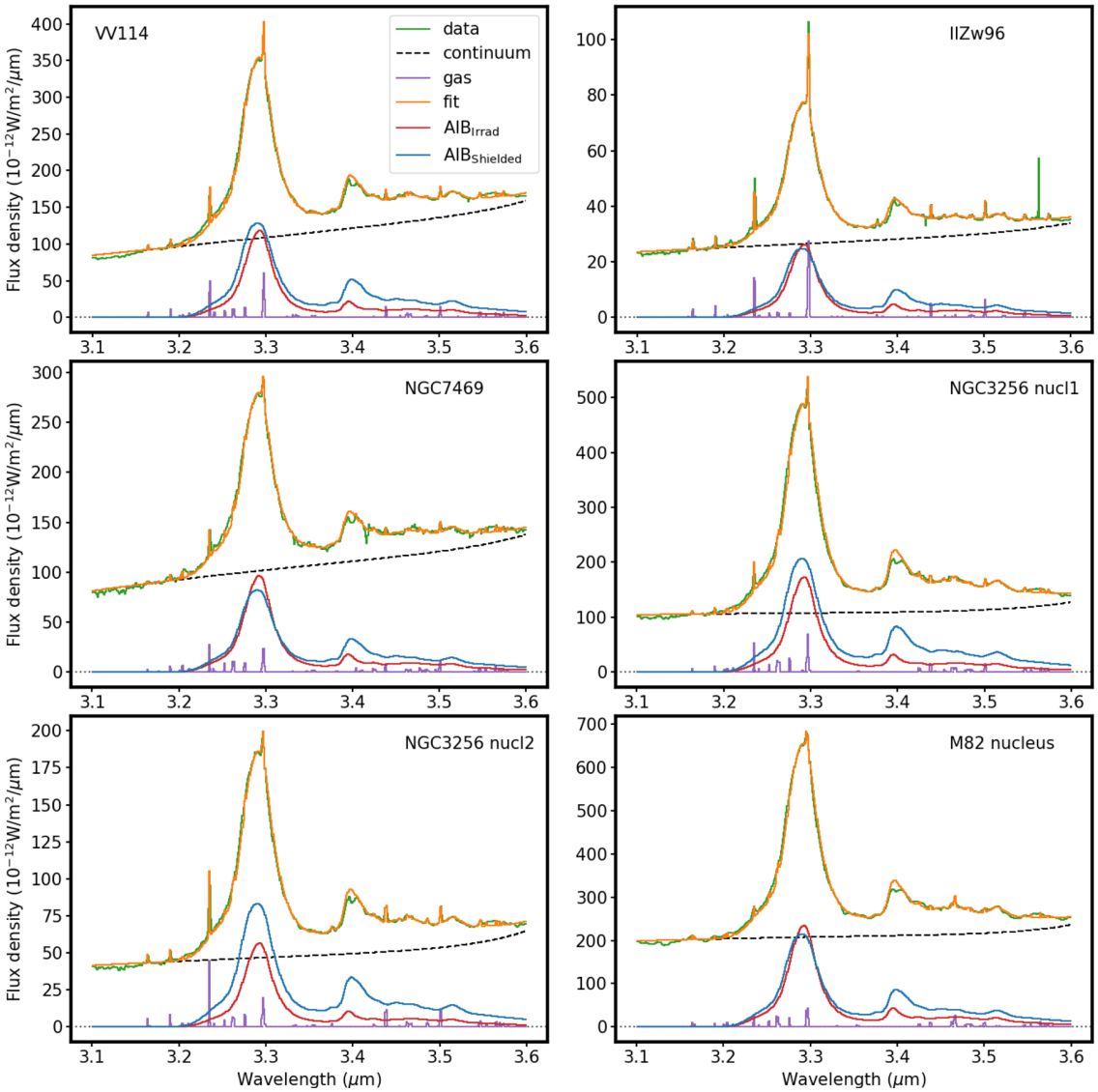

Fig. 5. ULIRGs from GOALS-JWST NIRSpec and M82 from NIRSpec MSA fitted spectra using a linear combination of continuum (dashed black lines), emission lines (purple solid lines), and the extracted templates AIB$_{Irrad}$ (in red) and AIB$_{Shielded}$ (in blue). Each panel corresponds to a galaxy whose name is indicated.

nucleus where both Paschen alpha and 3.3 μm emission peak. In NGC 7469, AIB$_{Irrad/Shielded}$ follows the knots of active star formation; however, the distributions are not fully co-spatial. Instead, it appears that AIB$_{Irrad/Shielded}$ is somewhat on the edges of these knots and seems to miss the star-forming region in the south. The situation near the nucleus is more difficult to assess due to saturation of the NIRSpec spectra. For NGC 3256 nucleus 1, AIB$_{Irrad/Shielded}$ peaks close to the peak of 3.3 μm and Paschen Alpha emission near the nucleus of the galaxy. However, the spatial pattern differs: AIB$_{Irrad/Shielded}$ shows a more diffuse emission, linked to the star-forming knots, but not completely co-located as in NGC 7469. Finally, in NGC 3256 nucleus 2, the distribution of AIB$_{Irrad/Shielded}$ seems completely unrelated to Paschen alpha or the 3.3 μm emission. We do see, however, as in all other galaxies, a peak of AIB$_{Irrad/Shielded}$ near a star-forming knot to the northwest of the field of view (Fig. 6). Comparing the AIB$_{Irrad/Shielded}$ to the HST visible images, it appears that low values of AIB$_{Irrad/Shielded}$ seem to correspond to dark regions of the HST images (Fig. 6), where visual extinction is high (i.e., regions with large amounts of molecular gas). In summary, AIB$_{Irrad/Shielded}$ does seem to be related to the radiative feedback from massive stars in the observed galaxies. As in the Orion Bar, this ratio is high in the vicinity of massive OB stars, and it is much lower in regions with higher extinction and larger molecular gas fractions. This is also compatible with the findings of Lai et al. (2020), who found a correlation between the 3.4/3.3 μm band ratio and the radiation field intensity, suggesting that an aliphatic (3.4) component is more prone to photo-destruction in an intense radiation environment.

4.3. Fitting a high-redshift AIB spectrum

In the last step of our analysis, we fit the AIB spectrum of the $z = 4.2$ galaxy SPT0418 obtained with MIRI using our template spectra. The result of this fit is shown in Fig. 7. Although the S/N is poor in this observation, this suggests that our extracted templates could be applied to a high-redshift galaxy. For this source, the H_2 lines are not detected; thus, we derive an upper limit for the ratios between the H_2 line intensity and I_{AIB} using the measured RMS noise at the wavelengths of the 2.12 and

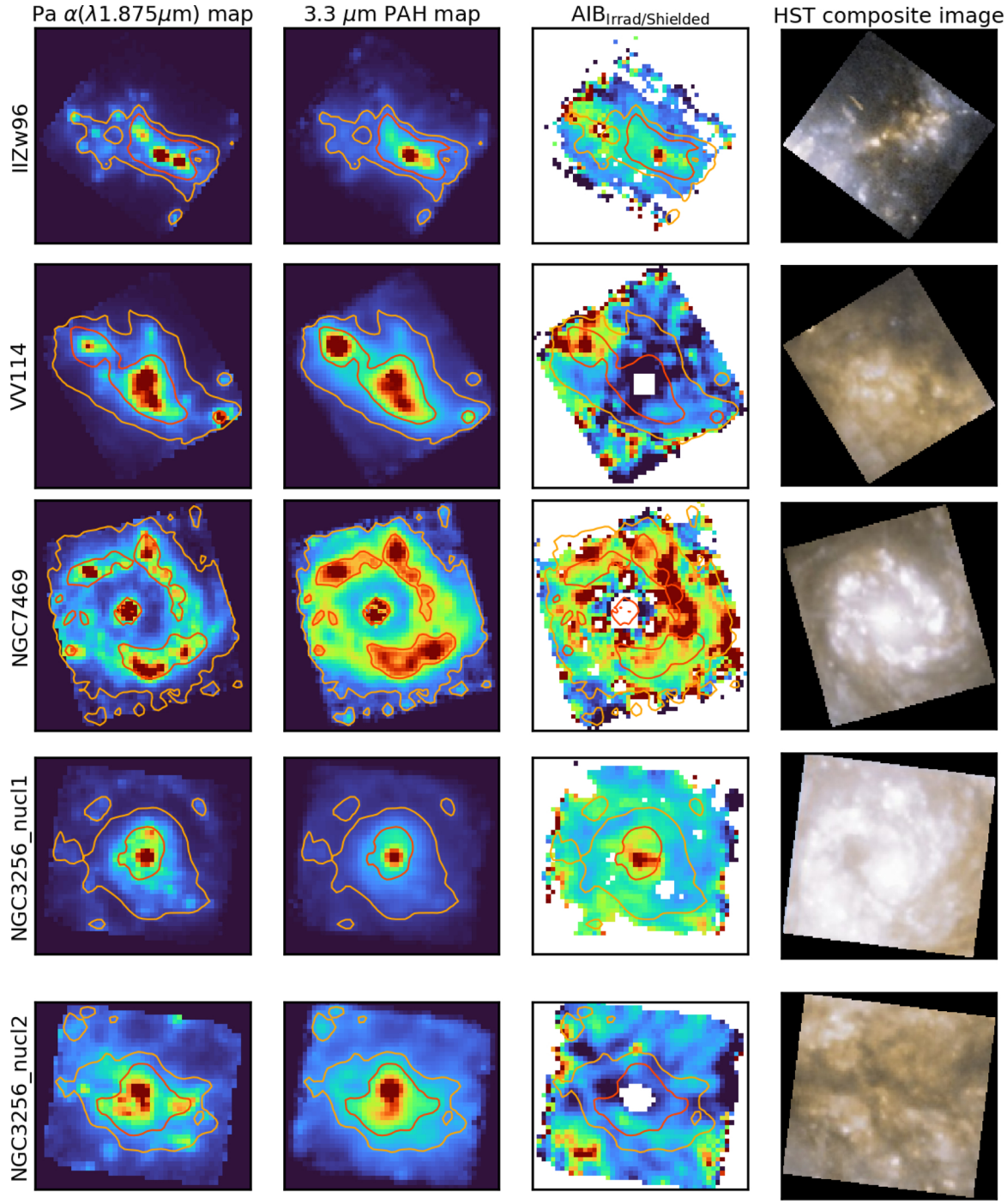

Fig. 6. GOALS-JWST galaxies emission maps and their AIB$_{Irrad/Shielded}$ spatial distribution. *First column*: NIRSpec continuum-subtracted Paschen α emission maps. *Second column*: NIRSpec continuum-subtracted 3.3 μm emission maps with intensity contours. The contours are shown in each panel for each galaxy for better comparison. *Third column*; AIB$_{Irrad/Shielded}$ contribution maps for each galaxy. In this column, saturated spaxels are represented in white. We note that we do not take into account edge spaxels as they are too noisy and mostly contain artifacts. *Last column*: *Hubble* Space Telescope color composite images ($F435W$ and $F814W$ filters) of each galaxy.

4.69 μm H_2 lines. We then place SPT0418 in the diagrams of Fig. 4. Interestingly, it appears to fall in a different region. While the H_2 over AIB ratio is only an upper limit, the AIB$_{Irrad/Shielded}$ is clearly lower than for nearby galaxies. This lower value of AIB$_{Irrad/Shielded}$ with respect to galaxies of the local Universe would indicate that less highly irradiated gas is present in SPT0418. This result is quite counterintuitive considering the large SFR of this galaxy. However, given the noisy nature of the spectrum (Fig. 7), the reliability of the derived value of AIB$_{Irrad/Shielded}$ needs to be confirmed with deeper observations of this source with MIRI.

5. Conclusion

In this work, using JWST NIRSpec observations of the Orion Bar, we extracted two template spectra, AIB$_{Irrad}$ and AIB$_{Shielded}$, which give a good representation of the AIB emission from this PDR in the 3.2–3.6 μm range. We show that the ratio

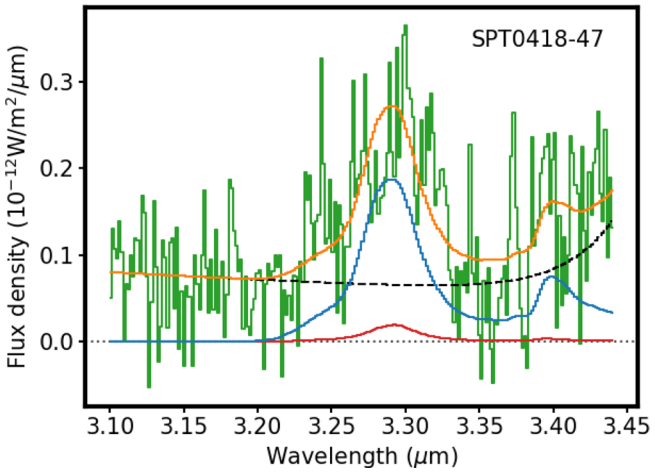

Fig. 7. Same as Fig. 1, but for the SPT0418 $z = 4.2$ galaxy using the extracted AIB_{Irrad} (fit shown in red) and $AIB_{Shielded}$ (fit shown in blue) templates.

between these two templates, $AIB_{Irrad/Shielded}$, is linked to the physical conditions in the PDR, with high values corresponding to regions where the UV field is strongest and where H_2 is dissociated and low values corresponding to regions where the UV field is weakest and where H_2 can form. We fit NIRSPec spectra of nearby galaxies using these two templates and extracted maps of the $AIB_{Irrad/Shielded}$ ratio. We showed that this ratio follows the radiative feedback from massive stars. Finally, we used our templates to fit the spectrum of a high redshift galaxy, showing the potential of such an approach to derive physical conditions of the ISM in these objects. These templates could also be used, for instance, to fit the spectral energy distribution of galaxies in order to constrain the intrinsic properties of galaxies such as their initial mass function distribution or even their SFR history. Additional spectroscopic observations with the JWST covering the range of the 3.3 µm AIB for both low- and high-redshift (up to $z \approx 7$) galaxies are needed to confirm and refine the potential of the approach presented here to determine the global physical conditions of the ISM in galaxies.

Acknowledgments. We thank the referee for her/his comments and suggestions which helped to improve the clarity of the manuscript. This work is based in part on observations made with the NASA/ESA/CSA *James Webb* Space Telescope. The data were obtained from the Mikulski Archive for Space Telescopes at the Space Telescope Science Institute, which is operated by the Association of Universities for Research in Astronomy, Inc., under NASA contract NAS 5-03127 for JWST. These observations are associated with programs #1288, #1328, #1355 and #2677. I.S., O.B., A.C. are funded by the Centre National d'Etudes Spatiales (CNES) through the APR program. E.P. acknowledges support from the University of Western Ontario, the Institute for Earth and Space Exploration, the Canadian Space Agency (CSA, 22JWGO1-16), and the Natural Sciences and Engineering Research Council of Canada.

References

Allamandola, L. J., Tielens, A. G. G. M., & Barker, J. R. 1989, ApJS, 71, 733
Armus, L., Lai, T., U, V., et al. 2023, ApJ, 942, L37
Bakes, E. L. O., & Tielens, A. G. G. M. 1994, ApJ, 427, 822
Basu-Zych, A. R., Lehmer, B. D., Hornschemeier, A. E., et al. 2013, ApJ, 774, 152
Berné, O., Joblin, C., Deville, Y., et al. 2007, A&A, 469, 575
Berné, O., Foschino, S., Jalabert, F., & Joblin, C. 2022a, A&A, 667, A159
Berné, O., Habart, É., Peeters, E., et al. 2022b, PASP, 134, 054301
Berné, O., Martin-Drumel, M.-A., Schroetter, I., et al. 2023, Nature, 621, 56
Bernstein, M. P., Sandford, S. A., & Allamandola, L. J. 1996, ApJ, 472, L127
Bianchin M., U V., Song, Y., Lai, T. S.-Y., et al. 2024, ApJ, 965, 103
Bohn, T., Inami, H., Diaz-Santos, T., et al. 2023, ApJ, 942, L36
Boulais, A., Berné, O., Faury, G., & Deville, Y. 2021, A&A, 647, A105
Chown, R., Sidhu, A., Peeters, E., et al. 2024, A&A, 685, A75
Draine, B. T., Dale, D. A., Bendo, G., et al. 2007, ApJ, 663, 866
Evans, A. S., Frayer, D. T., Charmandaris, V., et al. 2022, ApJ, 940, L8
Foschino, S., Berné, O., & Joblin, C. 2019, A&A, 632, A84
Habart, E., Peeters, E., Berné, O., et al. 2024, A&A, 685, A73
Habing, H. J. 1968, Bull. Astron. Inst. Netherlands, 19, 421
Inami, H., Surace, J., Armus, L., et al. 2022, ApJ, 940, L6
Joblin, C., Tielens, A. G. G. M., Allamandola, L. J., & Geballe, T. R. 1996, ApJ, 458, 610
Kim, J. H., Im, M., Lee, H. M., et al. 2012, ApJ, 760, 120
Lai, T. S. Y., Smith, J. D. T., Baba, S., Spoon, H. W. W., & Imanishi, M. 2020, ApJ, 905, 55
Lai, T. S. Y., Armus, L., U, V., et al. 2022, ApJ, 941, L36
Lai, T. S. Y., Armus, L., Bianchin, M., et al. 2023, ApJ, 957, L26
Lee, D. D., & Seung, H. S. 1999, Nature, 401, 788
Li, A. 2020, Nat. Astron., 4, 339
Linden, S. T., Evans, A. S., Armus, L., et al. 2023, ApJ, 944, L55
Marciniak, A., Joblin, C., Mulas, G., Mundlapati, V. R., & Bonnamy, A. 2021, A&A, 652, A42
McKinney, J., Pope, A., Armus, L., et al. 2020, ApJ, 892, 119
Morabito, L. K., Oonk, J. B. R., Salgado, F., et al. 2014, ApJ, 795, L33
Peeters, E., Habart, E., Berne, O., et al. 2024, A&A, 685, A74
Pilleri, P., Joblin, C., Boulanger, F., & Onaka, T. 2015, A&A, 577, A16
Rich, J., Aalto, S., Evans, A. S., et al. 2023, ApJ, 944, L50
Riechers, D. A., Pope, A., Daddi, E., et al. 2014, ApJ, 786, 31
Rigopoulou, D., Barale, M., Clary, D. C., et al. 2021, MNRAS, 504, 5287
Sakamoto, K., Aalto, S., Combes, F., Evans, A., & Peck, A. 2014, ApJ, 797, 90
Sandstrom, K. M., Koch, E. W., Leroy, A. K., et al. 2023, ApJ, 944, L8
Spilker, J. S., Phadke, K. A., Aravena, M., et al. 2023, Nature, 618, 708
U, V., Lai, T., Bianchin, M., et al. 2022, ApJ, 940, L5
Weingartner, J. C., & Draine, B. T. 2001, ApJS, 134, 263
Yamagishi, M., Kaneda, H., Ishihara, D., et al. 2012, A&A, 541, A10
Yang, X., & Li, A. 2023, ApJS, 268, 50
Yang, X. J., Li, A., Glaser, R., & Zhong, J. X. 2016, ApJ, 825, 22
Yang, X. J., Li, A., & Glaser, R. 2020, ApJS, 247, 1
Yoast-Hull, T. M., Everett, J. E., Gallagher, J. S., I., & Zweibel, E. G. 2013, ApJ, 768, 53
Yuan, C., Murase, K., & Mészáros, P. 2019, ApJ, 878, 76